DOI: 10.1002/ejic.201100344

New $BaM_2(SeO_3)_3{\cdot}nH_2O$ (M = Co, Ni, Mn, Mg; $n \approx 3$) Zemannite-Type Frameworks: Single-Crystal Structures of $BaCo_2(SeO_3)_3{\cdot}3H_2O$, $BaMn_2(SeO_3)_3{\cdot}3H_2O$ and $BaMg_2(SeO_3)_3{\cdot}3H_2O$

Magnus G. Johnston[a] and William T. A. Harrison*[a]

Keywords: Open frameworks / Zeolite analogues / Zemannite / Selenium / Ion exchange

The syntheses and characterisation of a new family of isostructural mixed-metal selenites based on the zemannite-type framework are described. These $BaM_2(SeO_3)_3{\cdot}3H_2O$ phases are built up from three-dimensional networks of MO_6 (M = Co, Ni, Mn, Mg) octahedra and SeO_3 pyramids. The octahedral groups form isolated M_2O_9 face-sharing pairs, which are linked by the selenite anions into a three-dimensional anionic framework. The framework encapsulates one-dimensional 12-ring channels occupied by the barium cations and water molecules. There are two types of channels: in one, the cations and water molecules are well ordered, and the channels are fully occupied; in the other, the same species are disordered, and the channels are partially occupied. There is little if any evidence of zeolitic reversible de/rehydration and cation ion-exchange behaviour for these materials.

Introduction

Zemannite, a mineral first found[1] in the Moctezuma mine (Sonora, Mexico) and named after the Austrian crystallographer Prof. J. Zemann, is the prototype phase for one of the most unusual families of inorganic open frameworks. Initially, there was some uncertainty over its chemical composition, and it was formulated as $Na_xH_yZnFe(TeO_3)_3{\cdot}nH_2O$.[2] A careful study by Miletech[3] indicated that magnesium, not sodium, is the extra-framework cation and that all of the framework iron atoms are trivalent, negating the requirement for extra-framework protons. Thus, zemannite, and the isostructural mineral kinichilite[4] (containing manganese in place of zinc), have ideal formulae of $Mg_{0.5}ZnFe(TeO_3)_3{\cdot}4.5H_2O$ and $Mg_{0.5}MnFe(TeO_3)_3{\cdot}4.5H_2O$, respectively. The zemannite framework is built up from MO_6 (M = Fe, Zn) octahedra and TeO_3 pyramids: isolated pairs of octahedra share a face as an M_2O_9 group, and the pyramidal tellurite groups link these units into a three-dimensional network encapsulating one-dimensional, 12-ring (i.e., 12 polyhedral building units; six MO_6 octahedra and six TeO_3 pyramids) channels. The Mg^{2+} ions and water molecules occupy these zeolite-like channels, but the $P6_3/m$ crystal (and channel) symmetry[3] means that the guest species must be highly disordered.

Various synthetic analogues of zemmanite have been prepared including $Na_2Zn_2(TeO_3)_3{\cdot}3H_2O$,[5] $Na_2Co_2(TeO_3)_3{\cdot}3H_2O$,[5] and the selenites $K_2Co_2(SeO_3)_3{\cdot}3H_2O$[6] and $K_2Ni_2(SeO_3)_3{\cdot}3H_2O$.[6] Some of these phases appear to show zeolitic behaviour of ion exchange (albeit very sluggish) and partial reversible dehydration without structure collapse.[5,6] A novel derivative of zemannite, $NaGa(TeO_3)_2{\cdot}2.4H_2O$[7] contains GaO_6 octahedra.

In this paper we describe our studies of a new family of zemannite-type selenite phases formulated as $BaM_2(SeO_3)_3{\cdot}3H_2O$ (M = Co, Ni, Mn, Mg), containing extra-framework barium cations. They adopt a new $2a \times 2a \times c$ superstructure of the zemannite aristotype,[8] which may possibly correlate with partial ordering of the extra-framework species in the 12-ring channels.

Results

Crystal Structures

$BaCo_2(SeO_3)_3{\cdot}3H_2O$ contains 29 non-hydrogen atoms (2 Ba, 4 Co, 6 Se, 17 O) in the asymmetric unit. Selected geometrical data are given in Table 1. The structure is shown in Figures 1 and 2.

There are four distinct Co atoms in this phase, all adopting octahedral coordination geometries, with d_{av}(Co1–O) = 2.144(4) Å, d_{av}(Co2–O) = 2.122(4) Å, d_{av}(Co3–O) = 2.146 (4) Å, and d_{av}(Co4–O) = 2.113 (4) Å, in satisfactory agreement with the ionic-radius sum[9] of 2.11 Å for Co^{II} and O^{-II}. These species fuse together through a face (as Co1 + Co2 and Co3 + Co4, respectively) to result in isolated $[Co_2O_9]$ units. For each CoO_6 group, the Co–O bonds involved in the octahedral face sharing (see Figure 1) are significantly longer than the "terminal" Co–O bonds (global mean values 2.184 Å and 2.078 Å, respectively). Co1 and Co2 are located on general positions, and Co3 and Co4 occupy (1/3, 2/3, z) special positions with site symmetry 3.

[a] Department of Chemistry, University of Aberdeen, Aberdeen, AB24 3UE, Scotland
E-mail: w.harrison@abdn.ac.uk

Table 1. Selected bond lengths [Å] and angles [°] for $BaCo_2(SeO_3)_3{\cdot}3H_2O$.

Ba1–O15^{i}	2.739 (4)	Ba1–O4	2.744 (5)
Ba1–O15	2.777 (4)	Ba1–O14	2.813 (4)
Ba1–O13^{i}	2.819 (4)	Ba1–O14^{i}	2.879 (4)
Ba1–O13	2.907 (5)	Ba1–O11^{ii}	2.925 (4)
Ba1–O10^{ii}	2.960 (4)	Ba2–O17^{iii}	2.405 (13)
Ba2–O16^{iv}	2.532 (14)	Ba2–O16^{v}	2.622 (15)
Ba2–O17^{vi}	2.807 (13)	Ba2–O7^{vii}	2.848 (5)
Ba2–O17^{iv}	2.900 (13)	Ba2–O8^{ii}	2.965 (5)
Ba2–O16^{iii}	2.966 (14)		
Co1–O7^{ii}	2.089 (5)	Co1–O6	2.109 (5)
Co1–O10	2.117 (5)	Co1–O2	2.148 (4)
Co1–O9	2.194 (4)	Co1–O11^{v}	2.207 (4)
Co2–O12^{viii}	2.061 (5)	Co2–O8^{v}	2.063 (5)
Co2–O4^{viii}	2.095 (5)	Co2–O2	2.145 (4)
Co2–O9	2.178 (4)	Co2–O11^{v}	2.187 (4)
Co3–O1^{ix}	2.091 (5)	Co3–O1^{x}	2.091 (5)
Co3–O1^{xi}	2.091 (5)	Co3–O5^{xii}	2.201 (4)
Co3–O5	2.201 (4)	Co3–O5^{xiii}	2.201 (4)
Co4–O3^{xii}	2.044 (4)	Co4–O3^{xiii}	2.044 (4)
Co4–O3	2.044 (4)	Co4–O5^{xii}	2.181 (4)
Co4–O5	2.181 (4)	Co4–O5^{xiii}	2.181 (4)
Se1–O1	1.675 (5)	Se1–O3	1.720 (5)
Se1–O2	1.727 (3)	Se2–O6	1.699 (5)
Se2–O4	1.720 (4)	Se2–O5	1.724 (3)
Se3–O7	1.685 (5)	Se3–O8	1.708 (5)
Se3–O9	1.728 (4)	Se4–O10	1.685 (5)
Se4–O12	1.717 (5)	Se4–O11	1.733 (4)
Se1–O1–Co3^{viii}	117.6 (2)	Se1–O2–Co2	115.6 (2)
Se1–O2–Co1	115.9 (2)	Co2–O2–Co1	84.38 (12)
Se1–O3–Co4	123.2 (2)	Se2–O4–Co2^{xi}	117.6 (2)
Se2–O5–Co4	115.3 (2)	Se2–O5–Co3	114.1 (2)
Co4–O5–Co3	82.24 (13)	Se2–O6–Co1	117.7 (2)
Se3–O7–Co1^{xiv}	119.8 (2)	Se3–O8–Co2^{vi}	118.2 (3)
Se3–O9–Co2	115.1 (2)	Se3–O9–Co1	114.7 (2)
Co2–O9–Co1	82.52 (13)	Se4–O10–Co1	118.1 (2)
Se4–O11–Co2^{vi}	114.8 (2)	Se4–O11–Co1^{vi}	114.1 (2)
Co2^{vi}–O11–Co1^{vi}	82.01 (12)	Se4–O12–Co2^{xi}	117.6 (2)

Symmetry codes: (i) $-x$, $1 + y$, $z - 1/2$; (ii) $x - y$, x, $z - 1/2$; (iii) $y - x$, $-x$, z; (iv) $-y$, $x - y$, z; (v) $x - y$, x, $1/2 + z$; (vi) y, $y - x$, $z - 1/2$; (vii) $-y$, $x - y$, $z - 1$; (viii) x, y, $z + 1$; (ix) $y - x$, $1 - x$, $z - 1$; (x) $1 - y$, $1 + x - y$, $z - 1$; (xi) x, y, $z - 1$; (xii) $y - x$, $1 - x$, z; (xiii) $1 - y$, $1 + x - y$, z; (xiv) y, $y - x$, $1/2 + z$.

The Co1···Co2 and Co3···Co4 separations are 2.8829 (9) Å and 2.8817 (18) Å, respectively, and the mean Co1–O–Co2 bond angle (contributors O2, O9, and O11) is 82.97°. The four selenium atoms (all on general positions) each have three O-atom neighbours in pyramidal coordination geometry, with typical geometrical parameters[10] for selenite groups [d_{av}(Se1–O) = 1.707(5) Å, θ_{av}(O–Se1–O) = 100.7(2)°, BVS(Se1) = 4.02; d_{av}(Se2–O) = 1.714 (5) Å, θ_{av}(O–Se2–O) = 100.8(2)°, BVS(Se2) = 3.89; d_{av}(Se3–O) = 1.707(4) Å, θ_{av}(O–Se3–O) = 101.2(2)°, BVS(Se3) = 3.98; d_{av}(Se4–O) = 1.707(4) Å θ_{av}(O–Se4–O) = 101.5(2)°, BVS(Se4) = 3.95]. In each case, we may assume that the fourth tetrahedral vertex is occupied by the unobserved Se^{IV} lone pair of electrons, at least in terms of the VSEPR model. Of the 12 framework O atoms in this phase, eight are dicoordinate to Co + Se (mean angle 118.7°) and four (O2, O5, O9, O11) are tricoordinate to two Co + one Se. All these tricoordinate species are parts of the shared face between two CoO_6 moieties.

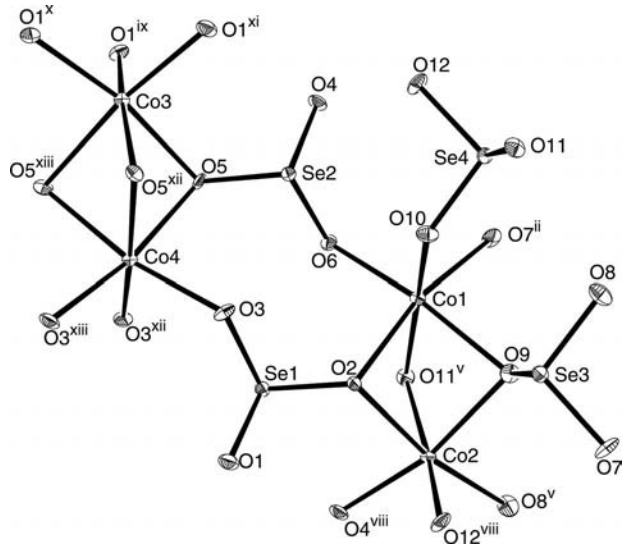

Figure 1. Framework atoms of $BaCo_2(SeO_3)_3{\cdot}3H_2O$ (50% displacement ellipsoids), with the structure expanded to show the full cobalt coordination polyhedra. For symmetry codes, see Table 1.

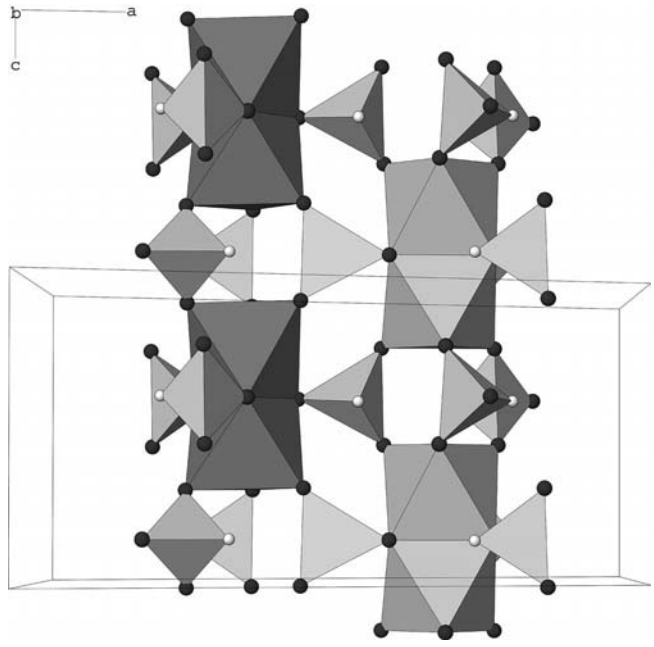

Figure 2. Polyhedral representation of a fragment of the framework of $BaCo_2(SeO_3)_3{\cdot}3H_2O$ viewed approximately perpendicular to (001) of the columns of face-shared octahedra linked by "lantern" motifs of three selenite groups; the same anions crosslink to adjacent octahedral columns displaced by $c/2$ in the z direction. The selenite groups are represented by pseudo tetrahedra, with the unshaded sphere representing the approximate location of the Se^{IV} lone pair of electrons.

The extra-framework species consist of two Ba^{2+} cations and five O atoms, assumed to be parts of water molecules. The species (Ba1, O13, O14, O15) in the first type of 12-ring [001] channels at $x = 1/2$, $y = 1/2$ and symmetry-equivalent locations (Figure 3) are well ordered, and the channels all are fully occupied within experimental error. The site occupancies of the species were therefore fixed to unity for the

final cycles of least-squares refinement. The Ba1 species (mean Ba–O 2.840 Å) is nonacoordinate to three framework and six extra-framework O atoms: the polyhedral geometry is irregular. Adjacent $Ba1O_9$ units in the channel share triangular faces through the three extra-framework water O atoms (O13, O14, and O15). Its bond valence sum (BVS) of 2.05 is in good accord with the expected value of 2.00.[11] The second [001] channel, at $x = 0$, $y = 0$ and equivalent locations possesses threefold crystallographic symmetry about its central axis, and the guest species (Ba2, O16, O17) cannot be placed without substantial disorder. In particular, every Ba2 cation has two symmetry-generated neighbours with the same z coordinate and with d(Ba···Ba) ≈ 2. 0 Å, and the channels cannot be more than 1/3 occupied. This was confirmed by a site-occupancy refinement for Ba2, which converged to 0.33 within experimental error and was fixed at that value for the final cycles of least squares. O16 and O17 [site occupancies 0.636(16) and 0.365(16), respectively (sum constrained to unity)] are also partially ordered, and the displacement factor for O16 is rather large. Allowing for the disorder, Ba2 is also nonacoordinate (mean Ba–O 2.780 Å).

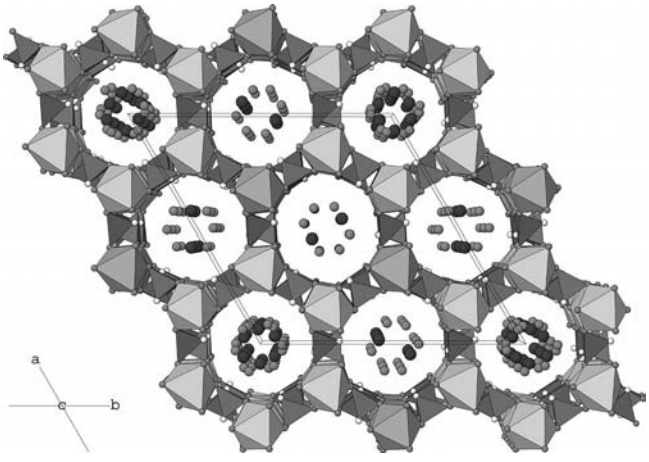

Figure 3. Unit-cell packing for $BaCo_2(SeO_3)_3{\cdot}3H_2O$ viewed approximately along [001] in polyhedral representation. The ordered (x = 1/2, y = 1/2) and disordered (x = 0, y = 0) 12-ring channels are apparent.

The polyhedral connectivity in $BaCo_2(SeO_3)_3{\cdot}3H_2O$ involves the SeO_3 moieties linking the Co_2O_9 octahedral pairs into a three-dimensional, anionic framework. The face-shared Co1/Co2 and Co3/Co4 octahedral pairs are each linked into [001] infinite columns by three bridging selenite groups (Figure 2) to form "lantern" motifs, somewhat akin to the way three tetrahedra link two octahedra in the NASICON structure.[12] This bonding *motif* uses two of the three Se–O vertices; the third vertex forms a crosslink to the central (shared) triangular plane of an adjacent octahedral pair, so that the octahedral pairs in any two adjacent columns are displaced by $\pm c/2$ or about ±3.8 Å in the c direction. As noted above, this Co/Se/O connectivity results in two types of infinite, one-dimensional 12-ring channels (Figure 3) propagating along [001], both about 7.35 Å in diameter (measured nucleus to nucleus). If the nominal O-atom radius of 1.4 Å is subtracted, the "free" channel diameter is about 4.55 Å. The extra-framework water molecules probably form O–H···O hydrogen bonds to the O atoms lining the channels, but no H atoms could be located in the present study. It is notable that the selenium lone pairs appear to point into the channels, which possibly impedes the mobility of the channel species.[13]

Crystal Structures of $BaMn_2(SeO_3)_3{\cdot}3H_2O$, $BaMg_2(SeO_3)_3{\cdot}3H_2O$, and $BaNi_2(SeO_3)_3{\cdot}3H_2O$

These are isostructural with their cobalt analogue, and their frameworks are essentially identical, allowing for slight size differences between these divalent ions. The extra-framework species appear to be almost the same for the manganese and magnesium phases. A partial refinement of the nickel phase seemed to indicate that *both* types of [001] channels are disordered, but this could be an artefact of the poor crystal quality. However, this does possibly correlate with the fact that the TGA results (vide infra) for $BaNi_2(SeO_3)_3{\cdot}3H_2O$ indicate a higher water content for the nickel phase. Full geometrical details for the structures are available as supplementary materials from the FIZ.

Thermal Analysis

The TGA trace for $BaCo_2(SeO_3)_3{\cdot}3H_2O$ (Figure 4) shows two reasonably well-defined weight losses (–7.9% between 120 and 450 °C and –29.1% between 470 and 620 °C; total loss –37%). A possible decomposition Scheme is as follows: $BaCo_2(SeO_3)_3{\cdot}3H_2O \rightarrow BaCo_2(SeO_3)_3 + 3\ H_2O$ gas (calculated weight loss 7.8%) → "$BaCo_2SeO_5$" + 2 SeO_2 gas (weight loss 32.1%). There appears to be another weight-loss step beginning around 930 °C, perhaps due to loss of further selenium as SeO_2.[14] The X-ray powder pattern of a sample heated to 400 °C shows two intense peaks (at 2θ = 28.2° and 33.5°) and a number of broader, less intense peaks, none of which could be matched to any reference patterns. The same sample heated to 700 °C gave a powder pattern with some peaks tentatively assigned to $BaSeO_4$ (JCPDS card 15-0374) and Co_3O_4 (JCPDS card 43-1003) indicating that some redox chemistry (oxidation of Se^{IV} to Se^{VI} and some of the Co^{II} to Co^{III}) may occur as the framework breaks down. A sample heated to 1200 °C in an alumina pan appeared to melt, as the alumina pan was found to be coated in an, as yet unidentified, greyish solid.

The TGA plot for $BaNi_2(SeO_3)_3{\cdot}nH_2O$ (Figure 5) has a profile similar to that of its Co congener. The first weight-loss step (11.4%) occurs between 150 and 500 °C, followed immediately by a second weight loss of 29.3% between 520 and 750 °C. Mass spectrometry indicated this first weight loss is composed entirely of water, indicating that the nickel phase must contain more extra-framework water than the cobalt phase. Based on a starting composition of $BaNi_2(SeO_3)_3{\cdot}4.5H_2O$, a possible decomposition pathway is:

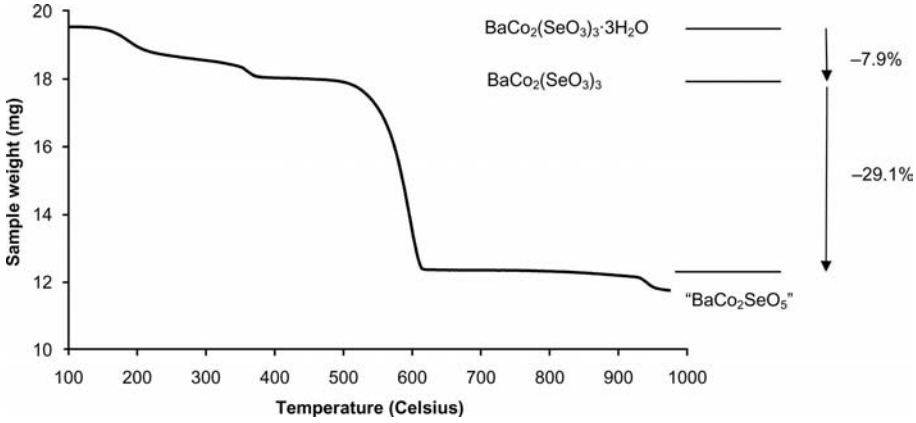

Figure 4. TGA trace for $BaCo_2(SeO_3)_3{\cdot}3H_2O$.

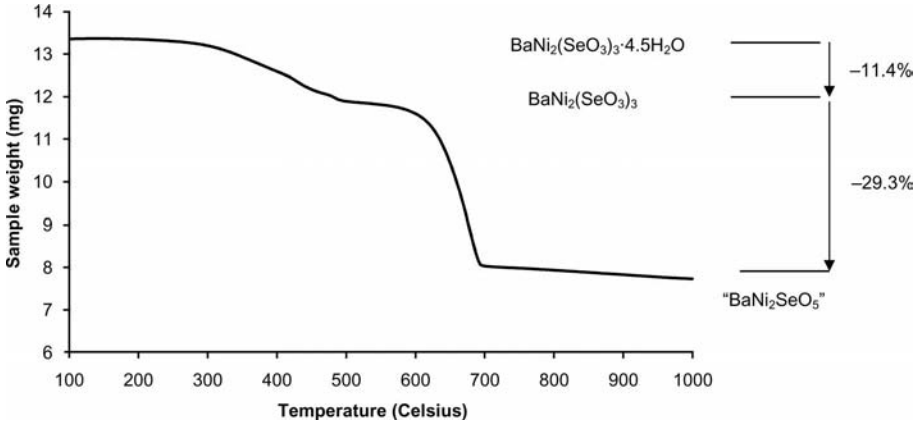

Figure 5. TGA trace for $BaNi_2(SeO_3)_3{\cdot}3H_2O$.

$BaNi_2(SeO_3)_3{\cdot}4.5H_2O \rightarrow BaNi_2(SeO_3)_3 + 4.5\ H_2O$ gas (weight loss 11.3%) → "$BaNi_2SeO_5$" + 2 SeO_2 gas (weight loss 20.9%).

Infrared Spectroscopy

The IR spectra of $BaCo_2(SeO_3)_3{\cdot}3H_2O$ and $BaNi_2(SeO_3)_3{\cdot}nH_2O$, as shown in Figure 6, are very similar. Both show a number of strong peaks in the 3550–2900 cm^{-1} range, which are typical of the symmetric and antisymmetric O–H stretching vibrations in water molecules. The relatively sharp peaks at 3530 cm^{-1} (Ni) and 3510 cm^{-1} (Co) are typical of weakly (ionically) bonded water molecules, and the broad peaks centred at 3165 and 2985 cm^{-1} (Ni), and 3175 and 3005 cm^{-1} (Co) are indicative of O–H···O hydrogen bonding: we can assume it must arise from either hy-

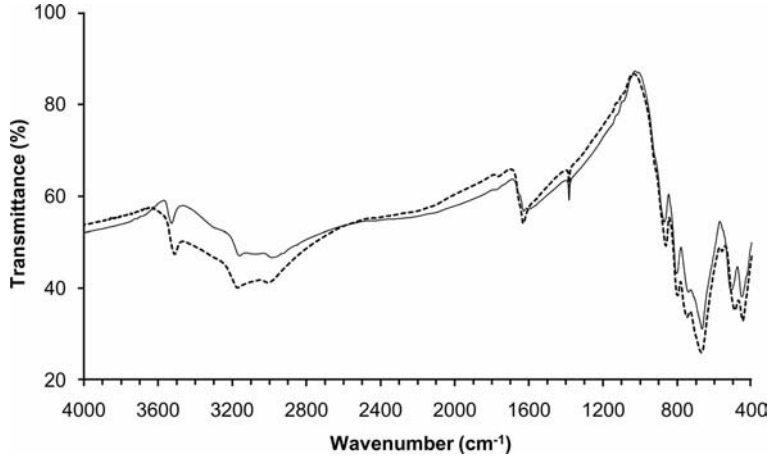

Figure 6. Overlaid IR spectra for $BaCo_2(SeO_3)_3{\cdot}3H_2O$ (dotted line) and $BaCo_2(SeO_3)_3{\cdot}3H_2O$ (continuous line).

drogen bonding between water molecules in the channels, or between the channel water molecules and the O atoms of the framework. The peaks at 1630 cm^{-1} (Ni and Co) can be assigned to H–O–H bending modes. The very intense, overlapping peaks in the 400–1000 cm^{-1} range are typical of Se–O and M–O (M = Co, Ni) stretching and O–Se–O bending modes seen in related compounds.[15]

De- and Rehydration Studies

Using the thermogravimetric analysis result as a guide, a 102.3 mg sample of $BaCo_2(SeO_3)_3{\cdot}3H_2O$ single crystals was heated to 240 °C under vacuum over a period of 8 h. During this time a weight loss of 2.9 mg (2.8%) was observed, corresponding to the dehydration of about 1.1 equiv. of H_2O in the formula. At this point, the oven was switched off, and water vapour was introduced into the vacuum line. During a period of 4 h, as the sample cooled to room temperature, just over 1.8 mg of water vapour was re-absorbed by the sample, indicating this first dehydration step is partially but not completely reversible. The same sample was then heated to 400 °C under vacuum overnight, thus almost completely dehydrating the sample. Once again, water vapour was introduced into the vacuum line, but no evidence for water uptake was observed as the sample cooled, apart from possible surface absorption effects. It was also seen that the colour of the single crystals had changed from purple to an intense deep purple, suggesting some redox chemistry had occurred (see above in the Thermal Analysis section) although the hexagonal crystal morphology remained. Attempts at single-crystal X-ray analysis of the resulting "crystals" gave frames of data with poorly defined, heavily smeared and unindexable spots, indicating that a severe structural collapse had occurred during the full dehydration step. This correlates with the poor quality powder patterns recorded for powders of $BaCo_2(SeO_3)_3{\cdot}3H_2O$ heated to 400 °C.

Figure 7 shows SEM images of the perfectly faceted hexagonal rods of $BaCo_2(SeO_3)_3{\cdot}3H_2O$ before dehydration. In the same Figure the devastating effect of the dehydration is

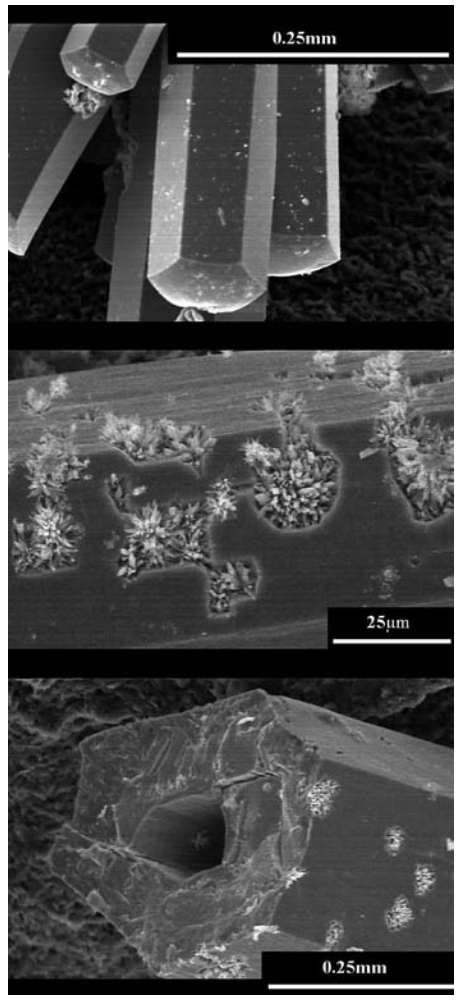

Figure 7. SEM views of $BaCo_2(SeO_3)_3{\cdot}3H_2O$ crystals before heat treatment (top), and after heating to 400 °C (center and bottom).

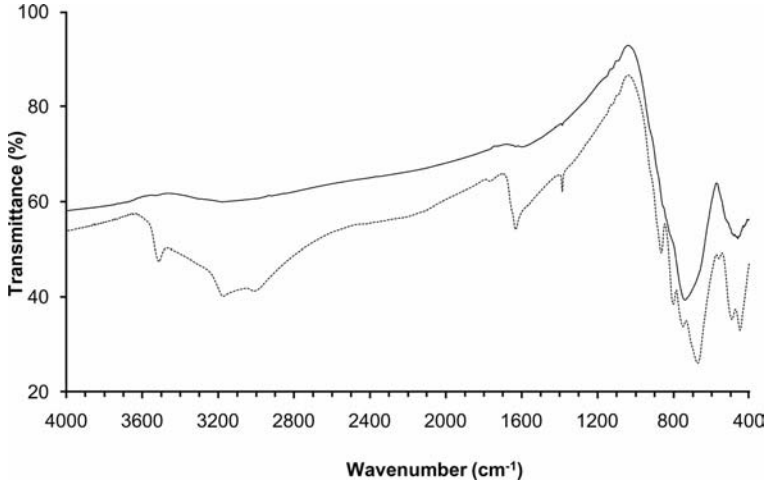

Figure 8. Overlaid IR spectra for $BaCo_2(SeO_3)_3{\cdot}3H_2O$ (dotted line) and dehydrated "$BaCo_2(SeO_3)_3$" (continuous line).

clearly demonstrated: "blast holes" in the sides and especially the ends of the hexagonal rods are apparent, indicating that water loss must occur with catastrophic structural failure.

The IR spectra of the fully hydrated and (almost) completely dehydrated samples of $BaCo_2(SeO_3)_3{\cdot}3H_2O$ are shown in Figure 8. The peaks associated with the water molecules (3550–2900 cm^{-1}, 1630 cm^{-1}) have almost disappeared in the dehydrated spectrum. The peaks associated with the framework have converged into two large broad peaks centred at about 750 and 420 cm^{-1}, again indicating a transition to a more amorphous state.

Ion-Exchange Studies

Flame tests on the powder products of reactions between $BaCo_2(SeO_3)_3{\cdot}3H_2O$ powder and $Sr(NO_3)_2$ solution indicated that little or no ion exchange had occurred, as the flame remained pale green, identical in colour with the unexchanged starting material. Although the analysis is rather crude, one would expect to see a significant red colourisation of the flame if a significant amount of Sr^{2+} had exchanged for Ba^{2+}.

$BaCo_2(SeO_3)_3{\cdot}3H_2O$ single-crystal ion-exchange experiments with lithium chloride solutions were more surprising. At 140 °C, the resulting crystals had undergone a grey discolouration and had dramatically "split" (similar to the way a tree-trunk might split when impacted lengthwise by an axe). Not surprisingly, all the crystals examined by single-crystal diffraction displayed multiple or smeared spots and could not be indexed. Whether any Li^+ ions have entered the channels in place of Ba^{2+} ions is difficult to say, but clearly a severe structural failure has occurred.

After 6 d of heat treatment at 80 °C in a sealed plastic bottle, the initially clear LiCl solution had turned blue, and rod-shaped crystals of a hue slightly bluer than that of $BaCo_2(SeO_3)_3{\cdot}3H_2O$ had appeared on the bottom of the bottle. Single-crystal X-ray diffraction revealed this new phase to be the structurally unrelated $Ba_2CoCl_2(SeO_3)_2$.[16] This can only arise because the $BaCo_2(SeO_3)_3{\cdot}3H_2O$ single crystals have dissolved in the LiCl solution and a new phase incorporating chloride ions has subsequently precipitated. The blue colour of the solution is presumed to be due to the presence of some tetrahedral $[CoCl_4]^{2-}$ (aq) ions.

Conclusions

The new phases $BaCo_2(SeO_3)_3{\cdot}3H_2O$, $BaMn_2(SeO_3)_3{\cdot}3H_2O$ and $BaMg_2(SeO_3)_3{\cdot}3H_2O$ have been prepared as single crystals by hydrothermal reactions. Single-crystal diffraction studies indicated these phases to be isostructural, apart from minor differences in the locations and occupancies of the extra-framework species. $BaNi_2(SeO_3)_3{\cdot}nH_2O$ almost certainly adopts the same framework structure, but intractable twinning problems prevented full structural elucidation.

The frameworks of these phases correspond to the topology of the zemannites noted in the Introduction section, in which face-sharing metal octahedra are linked by the pyramidal anions to form a three-dimensional framework encapsulating 12-ring channels occupied by the barium cations and water molecules. The unit cells seen here, with $a \approx 18$ Å and $c \approx 7.6$ Å correspond to a $2a \times 2a \times c$ supercell compared to the typical unit cells seen previously ($a \approx 9$ Å and $c \approx 7.6$ Å) for these types of materials, which might be accounted for by the ordered species in one type of [001] channel and the disordered species in the other. Conversely, all the channels are highly disordered in the $a \approx 9$ Å, $c \approx 7.6$ Å zemmanites.

Of the previously studied zemannite-related compounds, only $Na_2Zn_2(TeO_3)_3{\cdot}3H_2O$[5] has been shown to undergo ion exchange of the extra-framework species. Even then, the process is very sluggish, and is specific to Li^+: the reaction of $Na_2Zn_2(TeO_3)_3{\cdot}3H_2O$ with LiCl over a period of 10 d at 60 °C led to around 50% of Na^+ being exchanged for Li^+. Given the slightly smaller free diameter of the channels in $BaCo_2(SeO_3)_3{\cdot}3H_2O$ compared to the tellurite, coupled with the increased size of the extra-framework cations, it is perhaps not surprising that the degree of ion exchange in $BaCo_2(SeO_3)_3{\cdot}3H_2O$ seems to be extremely low. The complete dissolution of $BaCo_2(SeO_3)_3{\cdot}3H_2O$ in an LiCl solution and consequent formation of $Ba_2CoCl_2(SeO_3)_2$ is notable, however. It is also interesting that magnesium serves as a framework cation in $BaMg_2(SeO_3)_3{\cdot}3H_2O$ but is an extra-framework ion in zemannite. Further studies on these materials, including their magnetic properties, will be reported later.

Experimental Section

Syntheses

$BaCo_2(SeO_3)_3{\cdot}3H_2O$: $BaCO_3$ (0.1974 g, 1 mmol), $CoCl_2{\cdot}6H_2O$ (0.4759 g, 2 mmol), SeO_2 (0.3329 g, 3 mmol), and H_2O (10 mL) were sealed in an 18 mL capacity, Teflon-lined autoclave and heated to 150 °C for 4 d, followed by cooling to room temperature over 3 h. Product recovery by vacuum filtration and rinsing with water resulted in a nearly quantitative yield of purple hexagonal rods of $BaCo_2(SeO_3)_3{\cdot}3H_2O$.

$BaNi_2(SeO_3)_3{\cdot}nH_2O$: $BaCO_3$ (0.2961 g, 1.5 mmol), $NiCl_2{\cdot}6H_2O$ (0.7131 g, 3 mmol), SeO_2 (0.4993 g, 4.5 mmol), and H_2O (11 mL) were sealed in a 23 mL capacity, Teflon-lined autoclave and heated to 180 °C for 3 d, followed by cooling to room temperature over 3 h. Product recovery by vacuum filtration and rinsing with water resulted in a phase-pure product of pale-green hexagonal rods of $BaNi_2(SeO_3)_3{\cdot}nH_2O$ (yield ca. 95%).

$BaMn_2(SeO_3)_3{\cdot}3H_2O$: $BaCO_3$ (0.1974 g, 1 mmol), $MnCl_2{\cdot}4H_2O$ (0.3951 g, 2 mmol),0.5 M "H_2SeO_3" solution (dissolved SeO_2) (6 mL), and 1.0 M LiOH solution (4.5 mL) were sealed in an 18 mL capacity, Teflon-lined autoclave (starting pH = 8) and heated to 180 °C for 3 d, followed by cooling to room temperature over 3 h. Product recovery by vacuum filtration and rinsing with water resulted in very pale-pink hexagonal rods of $BaMn_2(SeO_3)_3{\cdot}3H_2O$ accompanied by brown and white powders [possibly hydrated $Mn(OH)_2$]. Reactions omitting the LiOH solution led to very pale-pink plates of the known phase $Mn_3(SeO_3)_3{\cdot}H_2O$.[17]

$BaMg_2(SeO_3)_3{\cdot}3H_2O$: This compound can be synthesised under both acidic and basic conditions. At low pH (ca. 2.5), $BaCO_3$ (0.597 g, 3 mmol), $Mg(NO_3)_2{\cdot}6H_2O$ (1.543 g, 6 mmol), SeO_2 (0.333 g, 3 mmol), and H_2O (15 mL) were sealed in a 23 mL capacity, Teflon-lined autoclave and heated to 180 °C for 3 d. Product recovery as above led to the isolation of an unidentified white powder and colourless hexagonal rods (maximum length ca. 0.5 mm) of $BaMg_2(SeO_3)_3{\cdot}3H_2O$. At higher pH (ca. 8), the reaction conditions and product recovery were the same as for the Mn phase, with starting materials as follows: $BaCO_3$ (0.197 g, 1 mmol), $Mg(NO_3)_2{\cdot}6H_2O$ (0.395 g, 2 mmol), 0.5 M "H_2SeO_3" solution (6 mL), and 1 M LiOH (aq) (4.5 mL). The resultant colourless needles (< 0.1 mm in length) were identified as $BaMg_2(SeO_3)_3{\cdot}3H_2O$ by comparison of the powder X-ray diffraction pattern with that of a simulated powder pattern generated from the single-crystal data. There were also a small number of peaks possibly corresponding to $Ba(OH)_2{\cdot}H_2O$ (JCPDS card 26-0154).[18]

Characterisation: Thermogravimetric analysis of the Co and Ni phases was carried out with a Mettler Toledo TGA/SDTA instrument from room temperature to 1000 °C, at a heating rate of 10 °C min^{-1} under air. A combined vacuum line/microbalance experiment was carried out on single crystals of $BaCo_2(SeO_3)_3{\cdot}3H_2O$ to assess the de/rehydration properties of the compound. During the experiment, around 100 mg of sample was heated under vacuum to partially dehydrate the compound. Water vapour was then reintroduced to the vacuum line (under atmospheric pressure). The weight loss/gain was monitored throughout the experiment by using the microbalance, and the reversibility of the de- and rehydration steps was assessed. The sample was then completely dehydrated in order to check the stability of the framework. Images of the fully hydrated and dehydrated single crystals were taken by using a Jeol JSM-5200 scanning electron microscope. Room-temperature infrared spectroscopy data for the Co and Ni congeners were collected with a Nicolet Nexus 670/870 FT-IR spectrometer. In both cases ca. 5 mg of sample was ground with ca. 200 mg of KBr and pressed into a thin pellet. Ion-exchange experiments were carried out on both powdered and single-crystal samples of $BaCo_2(SeO_3)_3{\cdot}3H_2O$. The powdered samples were mixed with 1 M solutions of $Sr(NO_3)_2$ and heated at 80 °C and 140 °C for anywhere between 3 d and 10 d. The reactions at 80 °C were carried out in PTFE bottles with stirring continuously on magnetic-stirrer hotplates. Reactions at 140 °C had to be carried out in autoclaves, thus preventing stirring. The resulting powders were then filtered and dried and flame tests carried out on the products. Based on the reported ion-exchange ability of similar compounds (see below), similar reactions were carried out with LiCl solution, but $BaCo_2(SeO_3)_3{\cdot}3H_2O$ was left in its single crystal form. The recovered crystals were then reanalysed by single-crystal X-ray diffraction. An X-ray powder pattern (Bruker D8 diffractometer, Cu-K_α radiation, λ = 1.54178 Å, T = 25 °C) for a ground portion of each sample was in good agreement with a simulation based on the appropriate single-crystal structure (see below) indicating phase purity and high crystallinity.

Crystal Structure Determinations: Suitable crystals [for $BaCo_2(SeO_3)_3{\cdot}3H_2O$, intense purple hexagonal rod, ca. $0.46 \times 0.09 \times 0.09$ mm; for $BaMn_2(SeO_3)_3{\cdot}3H_2O$, very pale-pink hexagonal rod, ca. $0.23 \times 0.05 \times 0.05$ mm; for $BaMg_2(SeO_3)_3{\cdot}3H_2O$, transparent hexagonal rod, ca. $0.22 \times 0.06 \times 0.06$ mm] were mounted on thin glass fibres with cyanoacrylate adhesive. Preliminary scans with a Bruker SMART 1000 CCD diffractometer (Mo-K_α radiation, λ = 0.71073 Å, $T = 20 \pm 2$ °C) indicated satisfactory crystal quality and a hexagonal unit cell with $a \approx 18$ Å and $c \approx 7.6$ Å in each case. For each phase, a hemisphere of intensity data was collected with the aid of the SMART and SAINT software packages.[19] Empirical (multi-scan) absorption corrections were applied by using SADABS[20] with resulting correction-factor ranges of 0.081–0.631 for $BaCo_2(SeO_3)_3{\cdot}3H_2O$ [22123 reflections scanned, 5186 unique (R_{Int} = 0.051), 4409 with $I > 2\sigma(I)$], 0.130–0.724 for $BaMn_2(SeO_3)_3{\cdot}3H_2O$ [18528 reflections scanned, 4350 unique (R_{Int} = 0.057), 3415 with $I > 2\sigma(I)$], and 0.143–0.741 for $BaMg_2(SeO_3)_3{\cdot}3H_2O$ [21871 reflections scanned, 5073 unique (R_{Int} = 0.065), 3494 with $I > 2\sigma(I)$]. Despite its well-developed hexagonal morphology, all the crystals examined of the nickel phase displayed multiple or smeared peaks. Data were collected on a green hexagonal rod of dimensions $0.31 \times 0.10 \times 0.10$ mm [a = 17.9263 (6) Å, c = 7.5204 (2) Å, V = 2092.92 (11) Å^3, 21669 reflections scanned, 4677 unique (R_{Int} = 0.036), 4009 with $I > 2\sigma(I)$], and a partial structural model was developed. The starting positional parameters for the heavy atoms and some of the O atoms in $BaCo_2(SeO_3)_3{\cdot}3H_2O$ were located by direct methods[21] in space group $P6_3$ (No. 173), and the remaining O atoms were located from difference maps as the full-matrix least-squares refinement against $|F|^2$ progressed. The simplest way to write the formulae of these compounds results in the rather unusual value of Z = 8 for this space group. Some of the extra-framework atoms are disordered (see below), and their site occupancies were allowed to vary. No hydrogen atom positions could be discerned in difference Fourier maps. The $BaMn_2(SeO_3)_3{\cdot}3H_2O$, $BaMg_2(SeO_3)_3{\cdot}3H_2O$, and $BaNi_2(SeO_3)_3{\cdot}nH_2O$ models were developed from that of the framework of $BaCo_2(SeO_3)_3{\cdot}3H_2O$ (Co replaced by Mn, Mg and Ni, respectively). In each case, the extra-framework species were located from difference maps and added to the model. Refinement of the Flack absolute

Table 2. Crystallographic parameters.

	$BaCo_2(SeO_3)_3{\cdot}3H_2O$	$BaMn_2(SeO_3)_3{\cdot}3H_2O$	$BaMg_2(SeO_3)_3{\cdot}3H_2O$
Empirical formula	$BaCo_2H_6O_{12}Se_3$	$BaH_6Mn_2O_{12}Se_3$	$BaH_6Mg_2O_{12}Se_3$
Formula mass	690.13	682.15	620.60
a [Å]	18.0430(6)	18.2683(8)	17.9840(8)
c [Å]	7.6120(2)	7.8329(3)	7.6140(3)
V [Å^3]	2146.08(12)	2263.86(16)	2132.63(16)
Z	8	8	8
Space group	$P6_3$ (No. 173)	$P6_3$ (No. 173)	$P6_3$ (No. 173)
T [°C]	20 ± 2	20 ± 2	20 ± 2
λ (Mo-K_α) [Å]	0.71073	0.71073	0.71073
$\rho_{calcd.}$ [g cm^{-3}]	4.272	4.003	3.866
μ [mm^{-1}]	16.92	15.34	14.14
Flack parameter	0.54 (2)	0.19 (3)	0.58 (3)
$R(F)$	0.034	0.039	0.047
$wR2(F^2)$	0.080	0.086	0.105

structure parameter[22] indicated that all the crystals studied were merohedrally (racemically) twinned. Except for $BaNi_2(SeO_3)_3 \cdot nH_2O$, the final difference maps were adequate, considering the disorder in some of the 12-ring channels. All crystallographic calculations were performed with SHELXL-97,[21] and details are summarised in Table 2. Further details of the crystal-structure investigations may be obtained from the Fachinformationszentrum (FIZ) Karlsruhe, 76344 Eggenstein-Leopoldshafen, Germany (Fax: +49-7247-808-666; E-mail: crysdata@fiz-karlsruhe.de), on quoting the depository numbers CSD-422872 [for $BaCo_2(SeO_3)_3 \cdot 3H_2O$], -422873 [for $BaMg_2(SeO_3)_3 \cdot 3H_2O$], and -422874 [for $BaMn_2(SeO_3)_3 \cdot 3H_2O$].

Acknowledgments

We thank Jim Marr and Brian Paterson for valuable assistance.

[1] J. A. Mandarino, S. J. Williams, *Science (Washington, DC)* **1961**, *133*, 2017.
[2] E. Matzat, *Tschermaks Mineral. Petrogr. Mitt.* **1967**, *12*, 108.
[3] R. Miletich, *Eur. J. Mineral.* **1993**, *5*, 176.
[4] M. Fleischer, *Amer. Mineral.* **1982**, *67*, 623.
[5] R. Miletich, *Monatsh. Chem.* **1995**, *126*, 417.
[6] M. Wildner, *Miner. Petrol.* **1993**, *48*, 215.
[7] N. H. P. Bhuvanesh, P. S. Halasyamani, *Inorg. Chem.* **2001**, *40*, 1404.
[8] H. D. Megaw, *Crystal Structures: a Working Approach*, W. B. Saunders, Philadelphia, **1973**, p. 216.
[9] R. D. Shannon, *Acta Crystallogr., Sect. A* **1976**, *32*, 751.
[10] W. T. A. Harrison, *Acta Crystallogr., Sect. C* **2005**, *61*, i76.
[11] N. E. Brese, M. O'Keeffe, *Acta Crystallogr., Sect. B* **1991**, *47*, 192.
[12] S. T. Norberg, *Acta Crystallogr., Sect. B* **2002**, *58*, 743.
[13] M. G. Johnston, W. T. A. Harrison, *J. Solid State Chem.* **2004**, *177*, 4680.
[14] V. P. Verma, *Thermochim. Acta* **1999**, *327*, 63.
[15] R. Rateesh, G. Suresh, V. U. Nayur, R. E. Morris, *Spectrochim. Acta* **1997**, *53*, 1975.
[16] M. G. Johnston, W. T. A. Harrison, *Acta Crystallogr., Sect. E* **2002**, *58*, i49.
[17] A. Larranaga, J. L. Mesa, J. L. Pizarro, R. Olazcuaga, M. I. Arriortua, T. Rojo, *J. Chem. Soc., Dalton Trans.* **2002**, 3447.
[18] W. Buchmeier, H. D. Lutz, *Z. Anorg. Allg. Chem.* **1986**, *538*, 131.
[19] *SMART* and *SAINT* software for area-detector diffractometer control, Bruker Analytical X-ray Systems, Madison, Wisconsin, USA, **1999**.
[20] G. M. Sheldrick, *SADABS*, program for scaling and correction of area detector data, University of Göttingen, Germany, **1997**.
[21] G. M. Sheldrick, *Acta Crystallogr., Sect. A* **2008**, *64*, 112.
[22] H. D. Flack, *Acta Crystallogr., Sect. A* **1983**, *39*, 876.

Received: March 31, 2011
Published Online: May 19, 2011

